JJEES
Jordan Journal of Earth and Environmental Sciences

Volume 9, Number 3, December, 2018
ISSN 1995-6681
Pages 185- 196

Characterization and Origin of Selected Basaltic Outcrops in Harrat Irbid (HI), Northern Jordan

Ali Al Smadi[1], Ahmad Al-Malabeh[2], Sana'a Odat[3*]

[1]Ministry of Education, Jerash, Jordan
[2]Department of Earth and Environmental Sciences, The Hashemite University, Zarqa, Jordan
[3]Department of Earth and Environmental Sciences, Yarmouk University, Irbid, Jordan

Received 19 October, 2018; Accepted 20 December, 2018

Abstract

This research is conducted to investigate the mineralogy, geochemistry and the petrology of Harrat Irbid (HI), in northern Jordan. Petrographic, mineralogical, and geochemical data were obtained from twenty representative samples selected from the studied HI outcrops. Mineralogical data show that HI consists of plagioclase, olivine, pyroxene, Feldspathoids, alkali feldspar, opaques, carbonates, iddingsite and chlorite minerals. The petrographical data show that the basalt is mesocratic and has hypocrystalline minerals. Modally, three petro-types are recognized, olivine-plagioclase- pyroxene phyric (23 %), olivine-pyroxene phyric (53 %) and olivine phyric basalt (24 %). The HI minerals are arranged mainly according to the porphyritic, glomeroporphyritic, paliotaxitic, vesicular, radiate and intergranular textures. Geochemically, all of the inspected samples of HI are located within plate alkaline basalt. They belong to the sodic series and are produced from undersaturated magma which resulted from a primitive mantle source. The rare-earth elements showed a depletion in the heavy rare earth elements and a strong negative Europium anomaly and enrichments in some lithophile elements, suggesting that the basalt resulted from a partial melting of a slightly differentiated pattern later. Magmas, which are analyzed for petrogensis modeling, may have been derived from low degrees (about 10 %) of partial melting of an enriched deeper garnet peridotite mantle source (>100km) with a limited crustal contamination.

© 2018 Jordan Journal of Earth and Environmental Sciences. All rights reserved

Keywords: Harrat Irbid, Porpheritic, Alkaline, Under-saturated, Mantle Source.

1. Introduction

Basaltic rocks cover approximately 18 % of Jordan's area (Fig. 1a). According to Bender, 1974; Al-Malabeh, 1993; and El-Hasan and Al-Malabeh, 2008, the basaltic rocks in Jordan occur as Harrat Al-Sham that emerge in the eastern and northern parts, and some eastern marginal basaltic occurrences (Fig. 1b) also appear in the Jordan Rift and central Jordan (Ibrahim et al., 2014).

Harrat Al-Sham is believed to be generated by a paleo-volcanic activity, accompanied by opening continental rifts since the beginning of the Oligocene and frequently in the Miocene, Pliocene and Pleistocene (e.g. Ibrahim, 1993; Ibrahim et al., 2001; Illani et al., 2001; Tarawneh et al., 2000).The results of this study can shed light on the span and duration of the upper-mantle upwelling beneath the western Arabian plate based on previous studies (Al-Amoush, 2010; Illani et al., 2001).

Basaltic rocks in the Jordanian Harrat cover about 11,400 km^2 (Al-Malabeh, 2009; Al-Oufi et al., 2012). The geology of Irbid area is an extension of south Syria's geology, and the samples taken from the area proved that the basaltic rocks exposed along the Irbid area are part of Harrat Al-Sham (Abu-Mahfouz et al., 2016; Al-Malabeh, 2009).

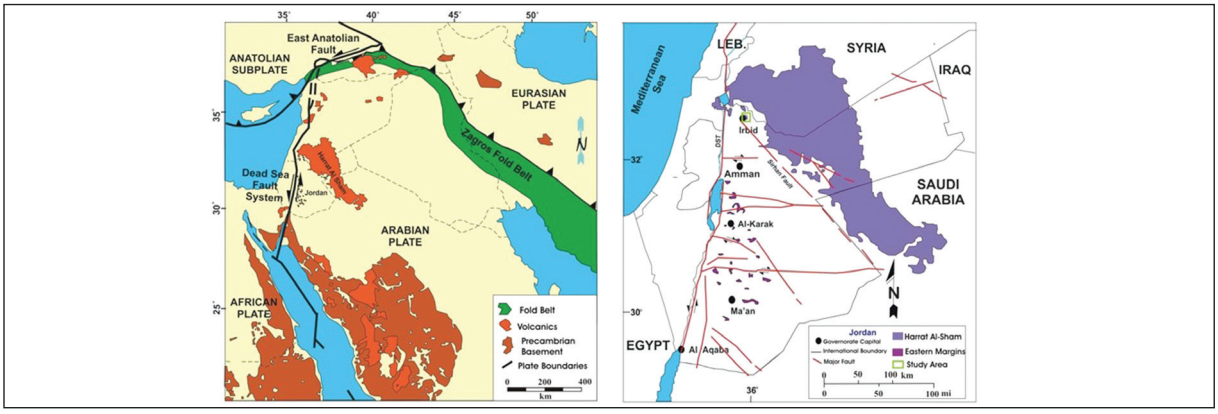

Figure 1. a. Location map of volcanic fields along the western Arabian plate (after Garfunkel, 1989; Camp and Roobol, 1989). **b.** Tectonic setting of Jordan and location of study area (Modified after Abed, 2000; and Ibrahim et al., 2014).

* Corresponding author. e-mail: sanaa.owdat@yu.edu.jo

2. Geology of Study Area

The study area geology characterized by sheet to gentle dipping and formation of wadis. The wadis resulted from head-way erosions formed by faulting and subsidence of the Dead Sea rift. The formation of this rift was followed by faulting, tectonic movements, and volcanic activity. The volcanic activity of HI is of the Pliocene to recent age and occurs as thick patches of basalt in the study area (Mo'hd, 1997).

Basaltic outcrops of the central parts of Irbid are located about 69km north of the Jordanian capital Amman; Irbid city is considered as one part of the study area. The study area lies between 35°48'40" to 35°55'41" longitude and between 32°31'30" to 32°36'36" latitude (Fig. 2). The basalt covers an area of about 10 Km^2 in NW-SE trend (Moh'd, 1997). Depending on the field survey, Geographic position system (GPS) and Google Earth images, seven HI's outcrops (Hw, Bu, Hk, DM, HZ, ST and DS) are shown on the location map (Fig. 2) to find out the spatial, mineralogical and geochemical relationships of basalt in the study area.

The slope of land, abundance of vesicular basalt and thicknesses of the basalt (Bryant, 1991) are evidences that the source of basalt comes from Irbid city and flows on to the surrounding low-lying areas (Fig. 2).

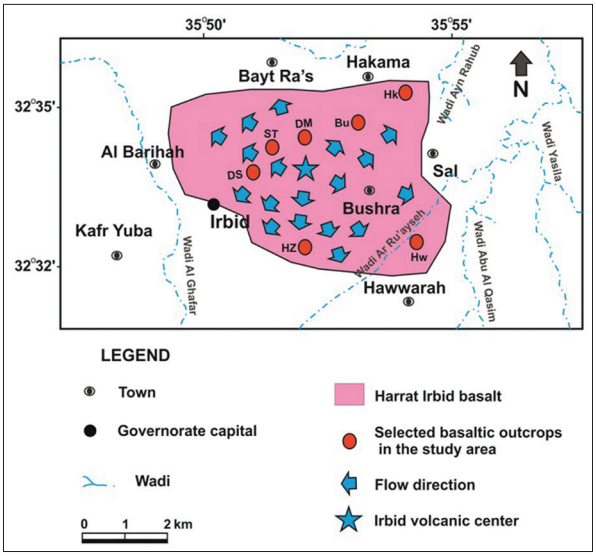

Figure 2. Location map of the study area showing that the selected basaltic outcrops and representative columnar sections will be correlated subsequently for these outcrops (Modified after Moh'd. 1997).

3. Sampling and Analytical Methods

Twenty fresh hand rock samples were collected randomly from different depths of HI outcrops for petrological, mineralogical and geochemical analyses. Three samples have been taken from DM, HZ, ST, DS, Hk & Hw, and two samples were taken from Bu basaltic outcrop. Fifty thin sections were prepared at the Department of Earth and Environmental Sciences at Yarmouk University and the Ministry of Energy and Mineral Resources (MEMR) for petrographic investigations. Seven microscopic slides were selected from each sample except DM, from which eight slides were taken. After preparation, they were evaluated using Leica Optical Microscope (LOM) and obtained using LEICA-DMEP Canon camera. After grinding approximately 100 g of each HI sample to a very fine powder using a crusher and a ring mill at the Institute of Earth and Environmental Sciences at Al al-Bayt University, they were dried at 90°C, and then powdered to be ready for analysis by X-ray fluorescence. X-ray fluorescence (XRF) analyses were carried out in the Jordan Atomic Energy Commission (JAEC) and at the Ministry of Energy and Mineral Resources (MEMR). XRF was used for the analysis of major and some trace elements (V, Ni, Zr and Zn) in the HI samples. Other trace elements can be defined by using Inductive coupled plasma (ICP) in MEMR. PetroGraph and Igpet softwares have been used to visualize, elaborate, and model the geochemical data for igneous petrology purposes.

4. Results

After studying thin sections under a microscope, the petrographic results of the HI samples from seven locations mostly indicate having the same texture (Aphanitic fine-grained rock, such as a basalt containing minerals that can't be distinguished with the naked eye). The basalt samples are characterized by a hypocrystalline texture which consists of a mixture of groundmass and crystals where the ratio of crystals to groundmass is greater than 3:5.

Olivine and augite form the main phenocrysts phases with small amounts of plagioclase phenocrysts (Table 1) in these rocks. Typically, three petro-types are recognized, Olivine- Plagioclase- Pyroxene Phyric Basalt (23 %), Olivine- Pyroxene Phyric Basalt (53 %) and Olivine Phyric Basalt (24 %).

Table 1: Texture and mineralogy of the Harrat Irbid basalt

Outcrop	Textures	Relative abundance of minerals	Relative abundance of phenocrysts
Hw	Porphyritic, Glomeroporphyritic, Vesicular, Amygdaloidal, Seriate, Paliotaxitic	Pl > Px > Ol	Ol
Bu	Porphyritic, Glomeroporphyritic, Ophitic & Sub-Ophitic, Seriate, Radiate, Paliotaxitic	Pl > Px > Ol	Ol > Px > Pl
Hk	Porphyritic, Glomeroporphyritic, Amygdaloidal, Vesicular, Embayment, Paliotaxitic	Pl > Px > Ol	Ol
DM	Porphyritic, Glomeroporphyritic, Sub-Ophitic, Seriate, Radiate, Paliotaxitic	Pl > Px > Ol	Ol > Px > Pl
HZ	Porphyritic, Glomeroporphyritic, Sub-ophitic, Vesicular, Seriate, Intergranular	Pl > Px > Ol	Ol > Px
ST	Porphyritic, Glomeroporphyritic, Ophitic & Sub-Ophitic, Seriate, Intergranular	Pl > Px > Ol	Ol > Px
DS	Porphyritic, Glomeroporphyritic, Amygdaloidal, Vesicular, Sub-ophitic, Intergranular	Pl > Px > Ol	Ol > Px

© 2018 Jordan Journal of Earth and Environmental Sciences . All rights reserved - Volume 9, (Number 3), (ISSN 1995-6681)

4.1.1 Plagioclase

Plagioclase minerals, which are generally small-microliths within the matrix phase, form 32-43 % of the basaltic rocks. They are often euhedral or suhedral in shape and rarely show zonation (Fig. 3a). Labradorite plagioclase is the most abundant phenocryst in the HI samples. The average extinction angle of all the samples ranges between (29° -32°).

4.1.2 Clinopyroxene

The Clinopyroxenes are the second dominant (18-27 %) mineral phase in the basalt. They have euhedral or subhedral crystal shape with olivine and plagioclase, and are observed in the microcrystalline matrix. The bluish red to violet-brownish clinopyroxene is characterized primarily by 35°-50° extinction angle and other optical properties such as; inclined extinction, higher birefringence and sector zoning (Fig. 3b).

4.1.3 Olivine

There are two generations of olivine in the HI samples. The first one is usually colorless to pale yellow in thin sections, displays a parallel extinction, fractures and a higher birefringence, and ranges from 0.5 to 1.5 mm in diameter. Olivine phenocrysts in the three petrotypes are euhedral to subhedral, tabular, fine-grained and fractured with embayment textures (Fig. 3c) produced from complete or partial alteration to iddingsite by hydration or oxidation processes. The second generation of olivine (Fig. 3d) is characterized by serpentined macrocrysts, and may be derived from small-volume ultramafic magmas.

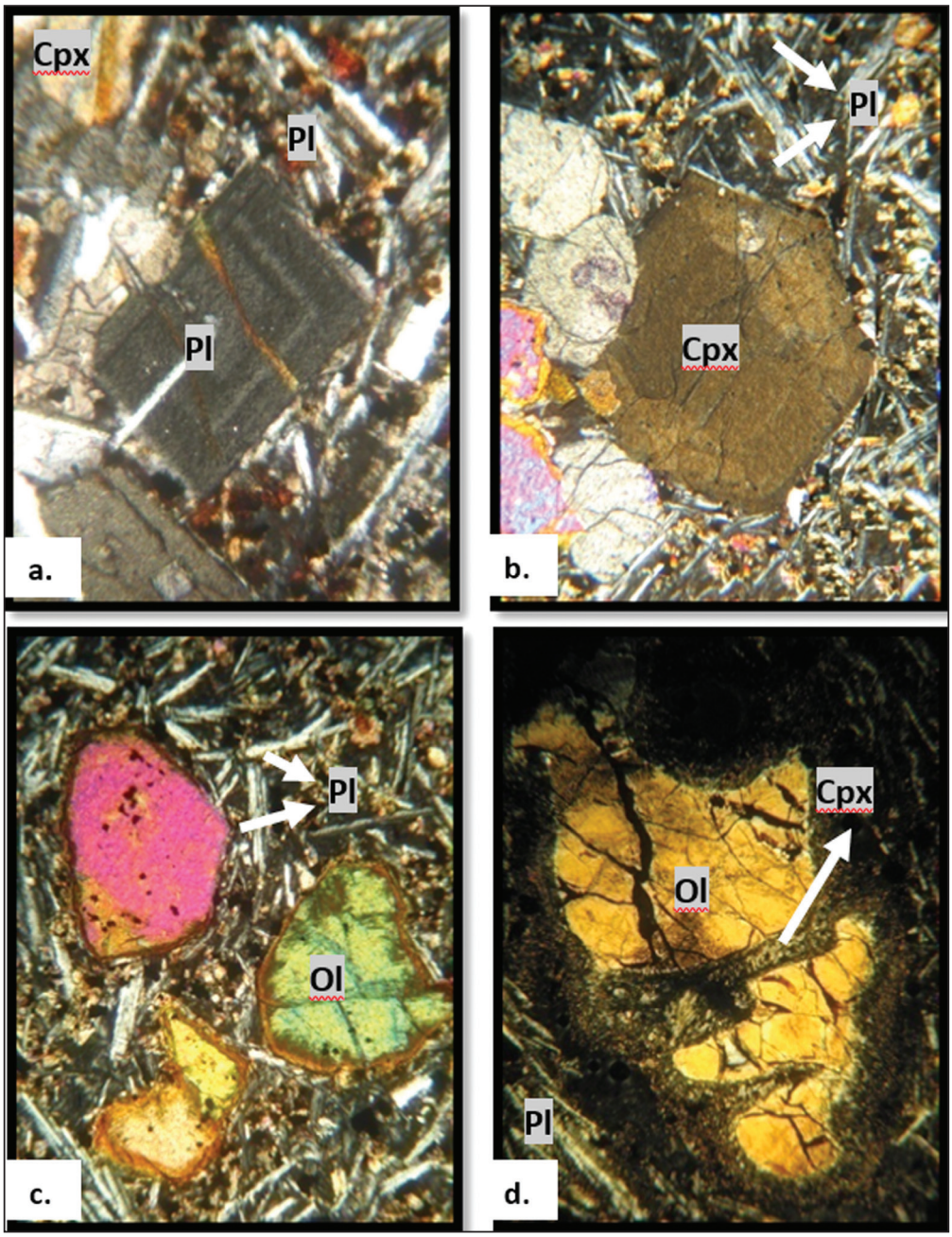

Figure 3. Photomicroscope images showing Oscillatory zoning of **a.** Plagioclase under XPL, 4x*10x magnification (Sample No. Hk1, 4x= 2.25 mm) and **b.** Clinopyroxene phenocryst, 10x*10x magnitude (Sample No. ST1, 10x= 1 mm). **c.** Photomicrograph showing porphyritic texture of three grains of olivine altered iddingsite on the rims within plagioclase and clinopyroxene groundmass under XPL, 10x*10x magnification (Sample No. DM1; 10x= 1mm). **d.** Photomicrograph image showing altered and serpentined olivine macrocryst surrounded closely by fine grained clinopyroxene groundmass under XPL, 4x*10x magnification (Sample No. DM2, 4x= 2.25 mm).

4.1.4 Accessory and Secondary minerals

Other accessory minerals include feldspathoids which consist of leucite (Fig. 4a) and nepheline (Fig. 4b), alkali feldspar (e.g. orthoclase) and magnetite, and secondary minerals such as carbonates, iddingsite and chlorite. The vesicles are filled with gas bubbles and carbonates.

The carbonate group is found to be calcite with a forth-order interference color (Fig. 4c), perfect cleavage and shows a pale red colour under PPL. It appears as a filling material, and the rock full of them can be called amygdaloidal texture.

4.1.5 Groundmass

The microcrystalline matrix is dominated by plagioclase, augite, olivine and magnetite. Two generations of microlites are apparent in the HI samples. One of these ranges in diameter between 0.15-0.34 mm and the other ranges between 0.4-0.6 mm due to disparity in the cooling rate.

4.1.6 Vesicles

Vesicles form when magmas generally continue to release gas, which can form bubbles inside; these bubbles get trapped in the solidified rock forming vesicles (Gill, 2010).

4.1.7 Textures

The HI minerals are arranged mainly by the porphyritic, glomeroporphyritic, paliotaxitic, vesicular, Amygdaloidal, sub-ophitic (Fig. 4d), radiate and intergranular textures.

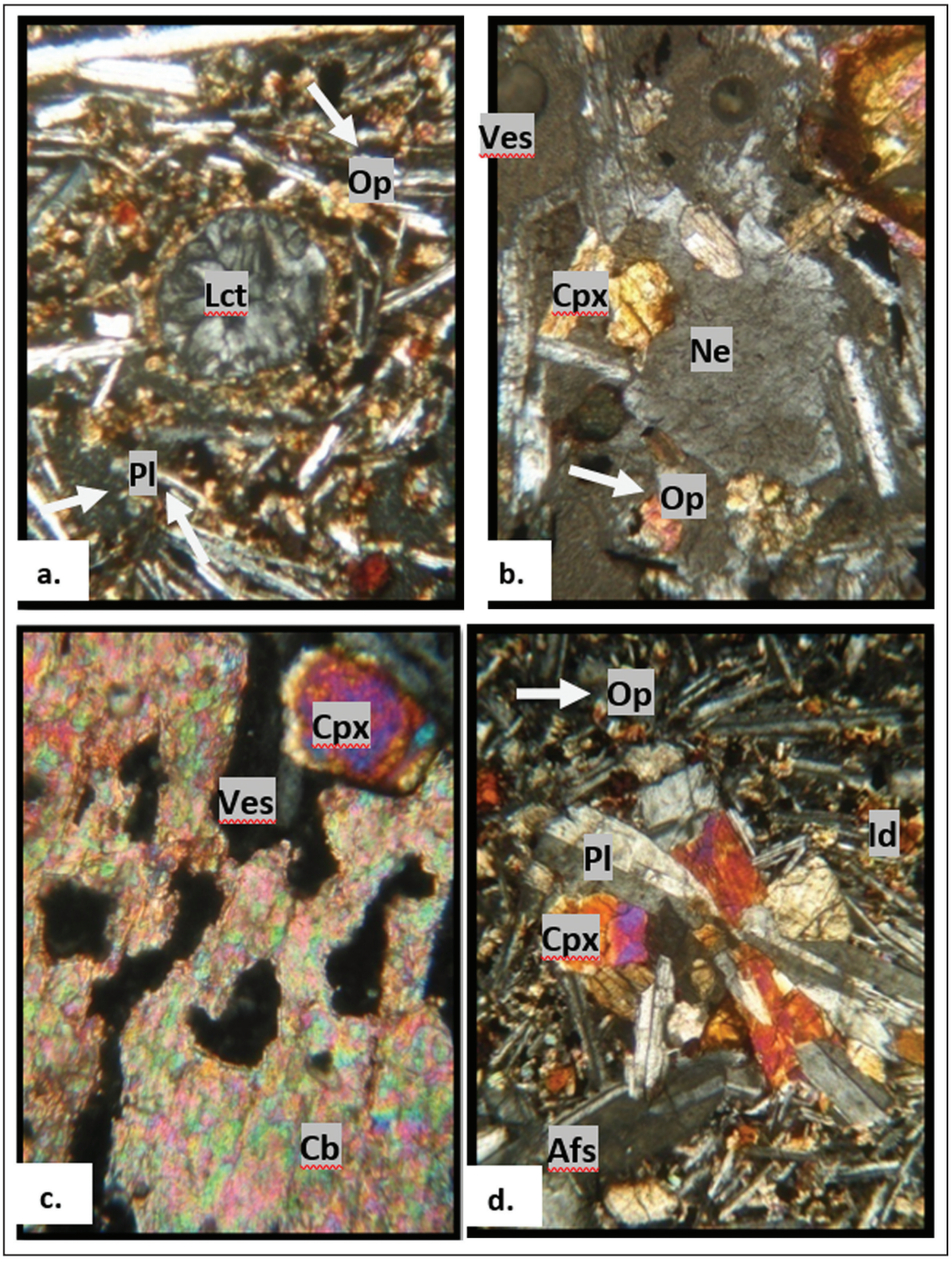

Figure 4. Photomicroscope images showing **a.** Euhedral leucite mineral enclosed within fine grain clinopyroxene groundmass under XPL, 4x*10x magnification (Sample No. ST1; 4x= 2.25 mm), **b.** Anhedral nepheline mineral under XPL, 4x*10x magnitude. (Sample No. DM1, 4x= 2.25 mm), **c.** Carbonates with a forth-order interference color filled the vesicles under XPL, 4x*10x magnification (Sample No. Hk2, 4x= 2.25), **d.** Clinopyroxene grains are incompletely within plagioclase phenocrysts (Sub-ophitic texture) under XPL, 10x*10x magnification (Sample No. Bu1, 10x= 1 mm).

Table 2. Major, trace elements and CIPW norm data for the HI basalt.

(wt%)	Hw1	Hw2	Hw3	Bu1	Bu2	Hk1	Hk2	Hk3	DM1	
SiO2	45.93	44.97	46.19	44.79	46.88	45.04	45.43	44.66	45.50	
TiO2	2.18	2.12	2.45	2.37	1.89	2.52	2.19	2.35	2.42	
Al2O3	14.37	14.09	15.64	15.29	14.75	15.86	14.29	15.20	15.80	
FeO(t)	11.06	11.14	11.36	11.46	11.36	11.40	11.36	11.38	11.53	
MnO	0.17	0.17	0.17	0.19	0.18	0.24	0.19	0.17	0.19	
MgO	7.19	7.02	6.07	6.43	7.32	4.54	6.85	5.80	6.77	
CaO	11.41	12.27	10.88	11.35	11.17	11.26	11.35	11.53	10.70	
Na2O	3.63	3.40	3.08	2.97	3.27	3.60	3.52	4.25	2.11	
K2O	1.15	1.09	1.23	1.10	0.69	1.21	1.21	1.05	1.02	
P2O5	0.32	0.33	0.32	0.46	0.42	0.40	0.30	0.37	0.38	
LOI	1.6	1.73	1.26	2.15	1	1.45	1.74	1.7	1.65	
Total	100.2	99.6	99.9	99.8	100.2	98.77	99.7	99.7	99.3	
Mg#	0.58	0.57	0.53	0.54	0.58	0.46	0.56	0.52	0.55	
Trace elements (ppm)										
V	264	259	278	293	245	315	244	269	248	
Cr	435	420	395	467	455	482	492	376	334	
Co	65	78	71	85	71	76	61	69	62	
Ni	200	185	177	189	180	169	182	190	222	
Cu	44	55	62	60	62	54	49	62	n.d.	
Zn	161	170	192	177	173	183	155	142	175	
Rb	18	21	20	18	17	17	17	19	19	
Sr	510	489	716	509	585	653	530	653	688	
Y	16	17	18	15	19	20	16	15	17	
Zr	161	96	124	188	131	103	174	110	199	
Nb	20	24	20	23	32	17	28	26	42	
Ba	127	418	49	908	473	619	816	138	229	
La	36	38	34	30	37	30	40	36	35	
Sm	9.2	7.1	6.6	8.6	7.8	6	6.4	5.7	6.4	
U	0.6	<12	<12	<12	0.6	<12	0.45	-	0.3	
Ti/Zr	80.7	131.6	117.7	75.1	86.0	145.8	75.0	127.3	72.5	
Zr/Nb	8.05	4.00	6.20	8.17	4.09	6.06	6.21	4.23	4.74	
K/Zr	59.3	94.25	82.34	48.57	43.72	97.52	57.73	79.24	42.55	
Y/Nb	0.80	0.71	0.90	0.63	0.59	0.65	0.71	0.62	0.41	
CIPW Norm (wt% normative)										
Or	6.8	6.44	7.27	6.5	4.08	7.15	7.15	6.2	6.03	
Ab	16.39	13.06	21	17.86	23.6	18.38	15.78	13.92	17.85	
An	19.55	19.99	25.26	25.19	23.56	23.57	19.65	19.33	30.63	
Ne	7.76	8.51	2.74	3.94	2.2	6.55	7.59	11.94	0	
Di	28.36	31.4	21.79	23.01	23.69	24.43	28.21	28.96	16.16	
Hy	-	-	-	-	-	-	-	-	9.99	
Ol	8.73	7.25	8.87	9.12	11.15	5.19	8.35	6.03	5.08	
Mt	5.34	5.38	5.48	5.54	5.48	5.51	5.48	5.5	5.57	
Il	4.14	4.03	4.65	4.5	3.59	4.79	4.16	4.46	4.6	
Ap	0.74	0.76	0.74	0.86	1.06	0.93	0.7	0.86	0.88	
An%	52.9	59.2	53.1	57.1	50	54.7	54	56.7	63.2	
C.I.	46.57	48.06	40.79	44.95	42.17	43.91	39.92	46.20	41.40	
D.I.	30.95	28.01	31.01	32.06	28.30	29.88	32.08	30.52	23.88	
S.I.	63.07	63.80	67.51	68.53	66.42	63.27	73.59	64.80	65.41	
R.S.	3.62	4.56	2.70	6.39	4.55	2.04	4.72	3.89	2.50	

	DM2	DM3	HZ1	HZ2	HZ3	ST1	ST2	ST3	DS1	DS2	DS3
	46.36	45.27	45.64	46.02	45.90	45.37	45.40	45.40	45.27	45.50	46.40
	2.18	2.43	2.22	2.17	2.22	2.20	2.18	2.19	2.22	2.40	2.19
	14.43	15.39	14.54	14.38	14.70	14.38	14.80	14.60	13.92	14.80	14.70
	11.04	11.72	11.09	11.11	10.81	11.05	10.99	10.81	11.34	11.08	10.72
	0.18	0.18	0.17	0.16	0.16	0.16	0.16	0.17	0.17	0.17	0.17
	7.45	6.45	7.19	7.40	7.74	6.15	7.01	7.01	7.00	6.58	8.19
	11.05	10.94	11.55	11.24	11.30	12.08	11.70	11.70	12.09	11.20	10.80
	3.49	3.24	3.52	3.56	2.96	3.75	3.07	2.99	3.66	3.56	3.05
	1.13	1.20	1.10	1.14	1.11	1.14	1.11	1.11	1.10	1.41	1.11
	0.31	0.34	0.34	0.29	0.35	0.33	0.31	0.32	0.34	0.42	0.31
	1.24	1.6	1.14	0.84	1.36	1.26	1.14	1.21	1.72	1.34	1.21
	100.1	100.1	99.7	99.5	99.8	99.1	99.1	98.7	100.1	99.7	100
	0.59	0.54	0.58	0.58	0.60	0.54	0.57	0.58	0.56	0.56	0.62
	270	256	262	248	200	275	215	214	314	223	223
	380	377	377	350	485	470	466	423	392	477	557
	78	55	69	56	52	72	60	53	78	136	94
	202	175	170	180	220	165	189	174	170	199	227
	46	65	52	47	50	55	42	42	47	70	50
	163	159	196	137	119	131	107	155	189	197	160
	20	20	18	21	20	17	18	18	19	20	18
	524	n.d.	537	528	628	520	566	589	499	634	616
	19	17	15	15	19	15	19	18	15	14	19
	216	200	227	212	164	171	166	145	180	191	191
	30	28	27	22	24	19	21	20	24	32	30
	463	348	222	258	285	366	401	184	280	264	275
	40	37	34	38	32	28	34	32	30	32	30
	8.3	8	5.6	6	6.2	8	7	7.4	7.1	6.6	7
	-	-	0.45	<12	<12	0.6	-	<12	0.4	<12	-
	60.1	72.4	58.3	61.0	80.7	76.7	78.3	90.0	73.5	74.9	68.3
	7.20	7.14	8.41	9.64	6.83	9.00	7.90	7.25	7.50	5.97	6.37
	43.43	49.81	40.22	44.64	56.19	55.34	55.51	63.55	50.73	61.28	48.24
	0.63	0.61	0.56	0.68	0.79	0.79	0.91	0.90	0.63	0.44	0.63
	6.68	7.09	6.5	6.74	6.56	6.74	6.56	6.56	6.5	8.33	6.56
	18.67	17.93	15.99	16.96	18.47	14.27	16.45	16.96	13.47	15.9	20.12
	20.4	23.94	20.65	19.92	23.55	19.07	23.32	23.14	18.33	20.24	23.14
	5.88	5.14	7.47	7.13	3.56	9.46	5.16	4.52	9.48	7.71	3.08
	26.27	22.97	27.93	27.55	24.32	31.51	26.39	26.47	32	26.32	22.82
	-	-	-	-	-	-	-	-	-	-	-
	9.93	9.45	8.85	9.44	10.9	5.69	9.03	8.89	7.25	8.11	12.21
	5.34	5.65	5.35	5.36	5.22	5.34	5.31	5.22	5.48	5.35	5.18
	4.14	4.62	4.22	4.12	4.22	4.18	4.14	4.16	4.22	4.56	4.16
	0.72	0.79	0.79	0.66	0.81	0.76	0.72	0.74	0.79	0.97	0.72
	52.2	57.18	56.36	54.02	56.04	57.19	58.64	57.7	57.64	56.01	53.49
	45.68	42.69	46.35	46.47	44.66	46.72	44.87	44.74	48.95	44.34	44.37
	31.23	30.16	29.96	30.83	28.59	30.47	28.17	28.04	29.45	31.94	29.76
	62.18	66.86	63.13	62.49	60.79	66.61	63.51	63.12	64.27	65.15	59.23
	2.75	3.91	3.50	3.11	2.80	4.12	3.48	3.42	4.19	3.98	2.45

4.2 Geochemistry

Major and trace elements and CIPW norm analyses (Table 2) are useful for the interpretation of geochemical and petrologic data trends. They can be used also to classify and name individual igneous rocks, a method that is useful for volcanic rocks which may have few identifiable minerals (Kelsey, 1965).

4.2.1 Biveriant Diagrams

Major element analysis (Table 2) is useful for the interpretation of geochemical and petrologic data trends and the classification of volcanic rocks. Basalt samples are classified to mesocratic basalt (with an average 45) defined by Colour Index [C.I. = Ol+ Hy+ Di+ Mt+ Il]. The Differentiation Index [D.I.= Q+ Ab+ Or+ Ne+ Kp+ Lc] of HI samples ranges from 24 to 32, and the Solidification Index [SI= 100 MgO / (MgO +FeO +Fe_2O_3 +Na_2O +K_2O) extends from 63 to 68 indicating a high fractionation of crystals of mafic minerals. The Rittmann Serial Index [R.S. = (Na_2O+ K_2O)*2/ (SiO_2 - 43)] (Rittmann, 1957 & 1962)) is used as a convenient petrochemical parameter to analyze the igneous rock series based on alkalinity: calcic- ($\sigma < 1.2$), calcalkaline- (1.2-3.5), alkaline- (3.5-8.8), and peralkaline-series (>8.8). Therefore, the Rittmann Serial Index of the HI equals at average ~3.62, and Indicates that they are located at the beginning of the alkaline phase.

The decrease in Fe_2O_3 and CaO as SiO_2 increases (Fig. 5) is consistent with the removal of early-forming plagioclase and/or pyroxene from the cooling magma. The samples have a relatively high FeO content, which may indicate small degrees of melting at high pressure (Wilson, 1989). Positive correlation between MgO and SiO_2 can be attributed to the low degree of the fractional crystallization temperature of olivine.

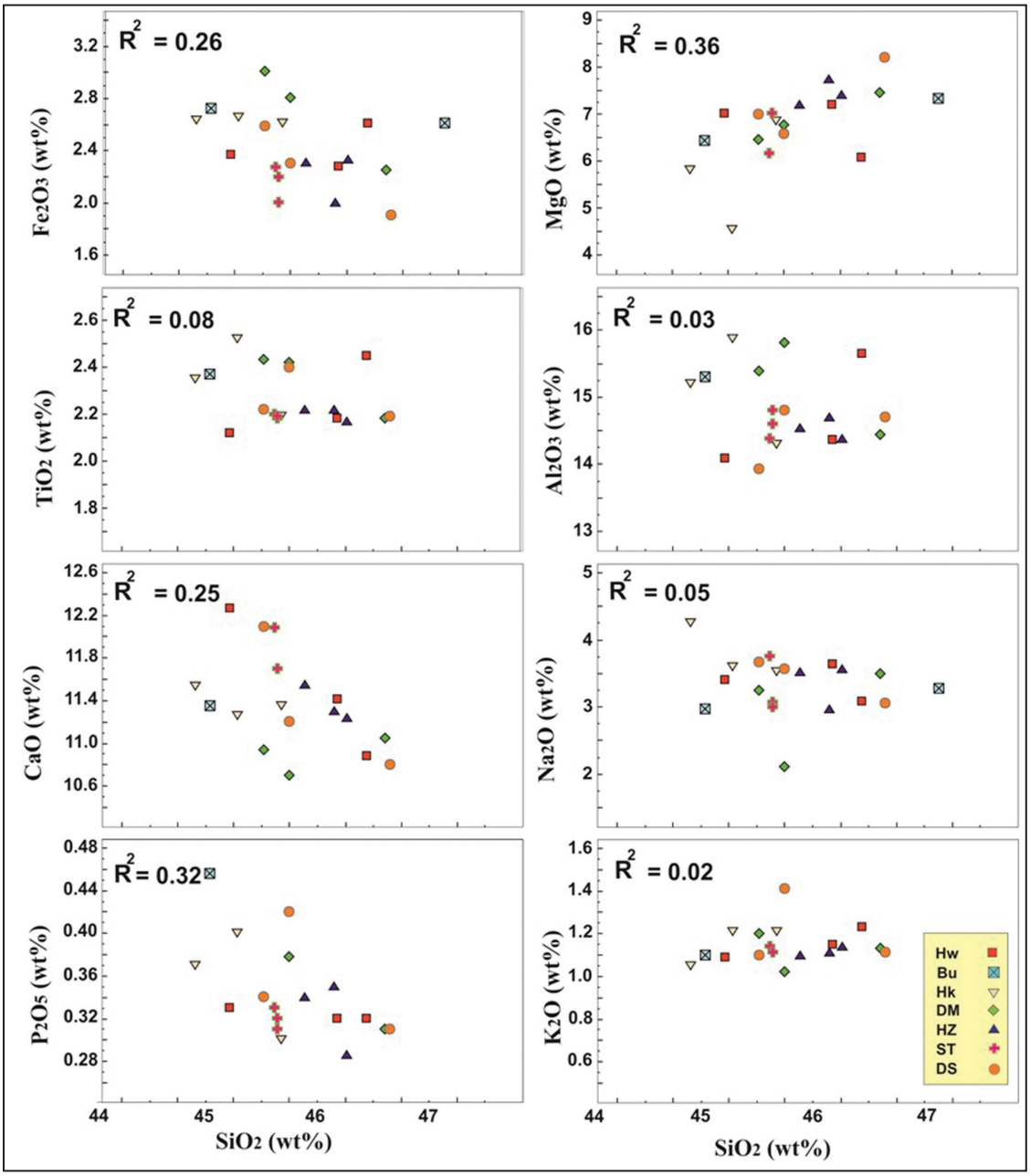

Figure 5. Harker variation diagrams for volcanic HI rocks. All major oxides are characterized by their unique trend as SiO_2 progresses from 44 – 48 wt %.

The Al_2O_3 curve shows a little negative to constant relation with SiO_2. Because CaO decreases continuously, these trends can be reconciled by speculating that clinopyroxene was removed early on removing Ca, but Al, and plagioclase began to crystallize later, removing both Ca and Al. The apparent constant to weakly- negative correlation of Na_2O and K_2O with SiO_2 indicates that the alkalies undergo two stages. First, the alkalies are not incorporated into crystallizing phase and are conserved in the magma. After that, the alkalies began to crystallize under low melting degrees, removing both K and Na.

At low SiO_2 concentrations, both TiO_2 and P_2O_5 raise systematically as neither oxide is incorporated in the early fractionating phases (e.g. olivine, Opx, or Ca-plagioclase), causing these two oxides to remain in the liquid phase. At lower temperatures, magnetite begins to crystallize and separate from the magma, causing the TiO_2 content of the remaining magma to drop suddenly. At lower temperatures, apatite begins to crystallize; resulting in another sharp kink in the P_2O_5 vs. SiO_2 plot.

Compatible elements of the HI samples include Ni, Cr, Co and Cu (Fig. 6). The Ni content ranges between 165 and 227 ppm with an average of 188 ppm, and indicates that the rocks suffered through very limited olivine fractionation. The copper lies between 42 and 70 ppm, with an average of 53 ppm.

The Cr, Ni and Co contents may also show the ancestry of the parental magma by the partial melting of a peridotite mantle source (Wilson, 1989). The Co/Mg ratio of the studied samples is relatively negative due to the incorporation of cobalt in the early precipitated Mg minerals. The Cu/Mg ratio in the studied samples is relatively negative compared with positive correlation of Cu/Fe and Cu/Na ratios. Thus, Cu/Fe and Cu/Na ratios should increase during fractionation and Cu substituting for Fe and Na in plagioclase and pyroxene (Alexander and Thomas, 2011).

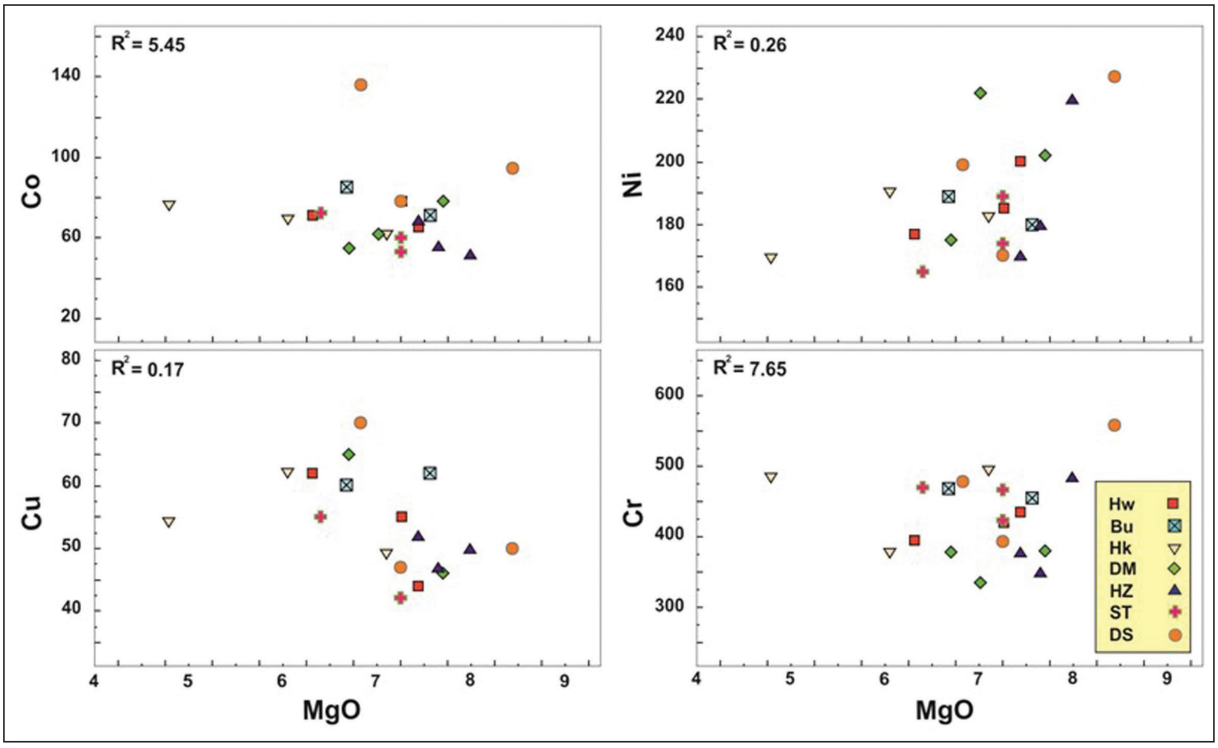

Figure 6. Variation diagrams showing compositional HI rocks ranges of selected major oxide (MgO) and compatible elements.

High-Field Strength (HFS) elements include Zr, Nb and Y (Fig. 7). The HI has a Zr content ranging from 110 to 191 ppm. The studied samples have high Ti/Zr and K/Zr averages of 59 and 85 ppm, respectively. Zr is a little positively correlated with K_2O in all samples, and it is independent with TiO_2 and P_2O_5. Zr/Nb ratio of HI is 6.7. The low Zr/Nb ratios of the HI samples are attributed to the source heterogeneities and the "enriched" nature of the source region (Pearce and Norry, 1979).

An average Zr/Nb value of 7 is given by Sunkel (1990) as a boundary between an alkaline and tholeiitic basalt, with the earlier investigated values of less than 7. Y contents show approximate constancy from 15 to 20 ppm in the HI with an average value of 17 ppm. The Y/Nb ratio averages 0.68. These ratios are appropriate with the ratio of <1 for intercontinental alkali basalts reported by Pearce and Cann (1973). The samples have high Zr/Y and Ti/Y ratios which average 10 and 825 in the samples respectively. The high Ti/Y ratio and the constancy of the Y content may indicate that the source magmas originated in garnet-bearing rocks (Frey et al., 1978).

4.2.2 Geochemical Classification of HI Volcanic rocks

Based on TAS diagram that is modified and recommended by Le Base et al. (1986), the typical evolutionary sequence (Fig. 8a) in the alkaline series of the HI rocks starts with an alkali olivine basalt, and proceeds to become alkali trachybasalt and tephrite basanite (Winter, 2001). Most of the HI samples fall in the alkali rocks region depending on the discrimination line of alkali and subalkalie rock fields after Irvine and Baragar (1971).

The alkaline and subalkaline rocks, when plotted on Ne-Ol-Qtz diagram (Fig. 8b) using the normative minerals

© 2018 Jordan Journal of Earth and Environmental Sciences . All rights reserved - Volume 9, (Number 3), (ISSN 1995-6681)

include nepheline, olivine and quartz, are marked by the dividing line that is close to the critical plane of silica undersaturation (Proposed by Irvine and Baragar, 1971). The HI samples fall in the undersaturated area.

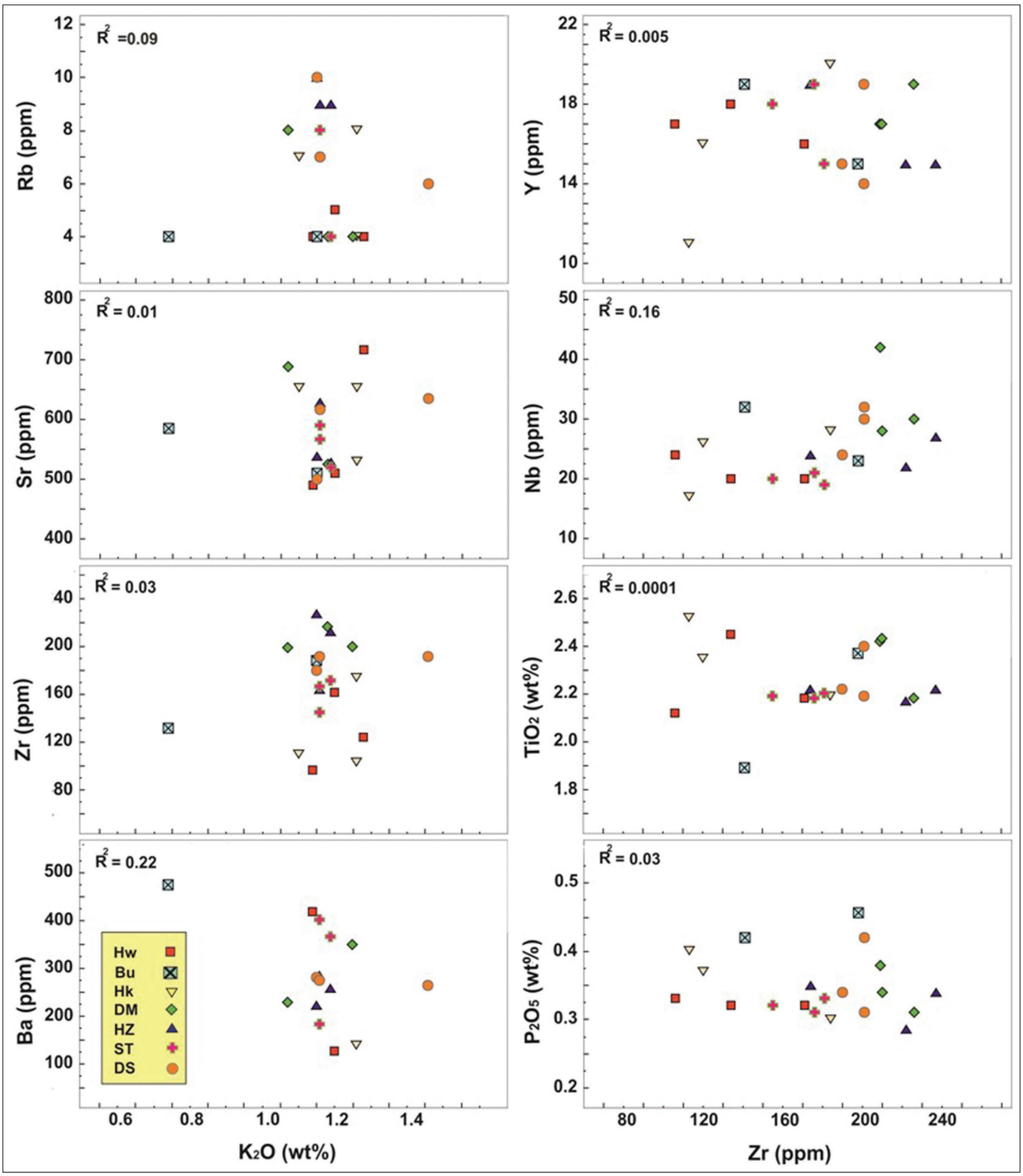

Figure 7. Variation diagrams showing interelemental relationships of the incompatible elements in the studied rocks.

The Nb/Y ratio (Fig. 8c) was first noted as an indicator of alkalinity in basalts by Pearce and Cann (1973), and further studies confirmed this (Floyd and Winchester, 1975); a higher Nb/Y (averages 1.5 in the HI samples) ratio generally reflects the higher Nb content characteristic of alkaline suites (Winchester and Floyd, 1976).

Using the K_2O versus Na_2O subdivision (After Middlemost, 1975) for alkaline magmatic rocks (Fig. 8d), the HI samples have high Na_2O/K_2O ratios; therefore, they belong to the Na-series of alkaline magmatism. This reflects a high albite and feldspathoidal content of these samples.

4.2.3 REE Diagram

The REE diagram normalized to Chondrite-Nakamura (1974) for the HI rocks (Table 3) shows depletion in the heavy rare-earth elements relative to the light ones and a strong negative Eu anomaly (Fig. 9). The HI samples with high abundances of lithophile elements and negative Eu anomalies represent fractionated melts which indicates that the basalt resulted from partial melting with slight differentiation (Anand and others, 2006). The positive relation between total abundance of REE and of other incompatible elements, which may reflect a lower degree of partial melting (Al-Malabeh, 1994).

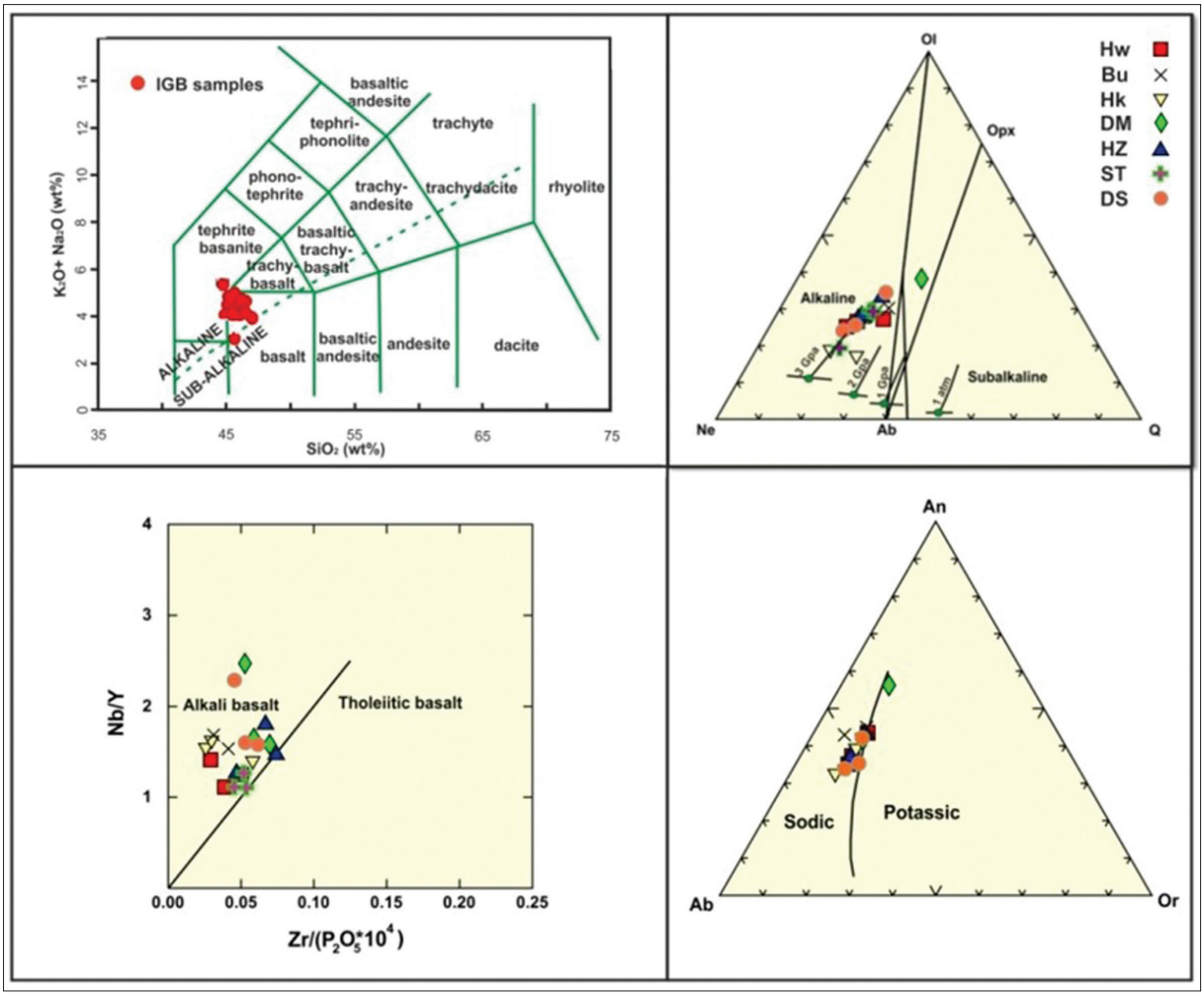

Figure 8. a. Chemical classification and nomenclature of the HI rocks using the total alkali versus silica (TAS) diagram (Le Base et al., 1986). The discrimination line of alkali and subalkalie rock fields after Irvine and Baragar (1971). **b.** A Ne-Ol-Q base of the basalt tetrahedron illustrating the compositions of the HI samples in highly undersaturated alkaline field (Modified after Irvine and Baragar, 1971). Change in the first melt composition with increasing pressure projected onto the base of the basalt tetrahedron (Modified after Kushiro, 1968). **c.** Zr/ (P_2O_5 *10^4) vs. Nb/Y diagram (After Winchester and Floyd, 1976). **d.** Normative An–Ab–Or diagram showing the sodic and potassic series of alkaline HI samples (After Irvine and Baragar, 1971).

Table 3. The average of REE-element concentrations in the studied HI outcrops (in ppm).

REE	Hw	Bu	Hk	DM	HZ	ST	DS
La	36	36	34	37	35	32	31
Ce	90	75	82	100	96	81	98
Pr	8.9	9.4	7	9	10	10.1	8.8
Sm	9.2	8.6	6.4	8	5.6	7	7.1
Eu	1.1	0.6	1	0.8	0.9	0.7	0.8
Gd	6.6	7.1	8	5.8	6.2	7	6.4
Dy	5.9	5.1	5.2	6.6	7.1	5.7	6.8
Er	3.2	3.9	3.4	2.9	4.2	3.8	3
Yb	1.75	1.9	1.5	1.7	1.3	1.42	1.2
Lu	0.25	0.18	0.15	0.2	0.17	0.15	0.18

4.2.4 Spider Diagram

The normalized trace elements Rb, Ba, U, K, Nb, La, Ce, Sr, P, Zr, Ti and Y spider diagram (Fig. 10) are normalized to the primordial mantle values of Wood et al. (1979) and plotted on a logarithmic scale. The normalized trace elements of the rock/primitive mantle shows a positive Nb peak, which is a good indicator that HI is a product of the asthenospheric part of the mantle rather than the lithospheric part (Al-Malabeh, 1994; Wilson, 1989).

The Zr and Sr anomalies can be illustrated in selective enrichment of the mantle source regions from which the primitive basalts were borrowed (Al-Malabeh, 1994).

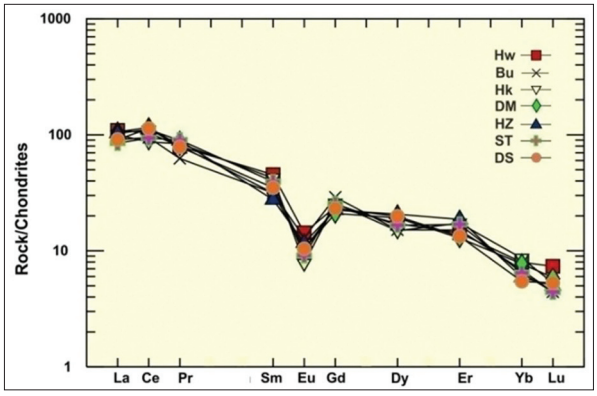

Figure 9. Chondrite normalized (Nakamura, 1974) REE patterns for the HI samples.

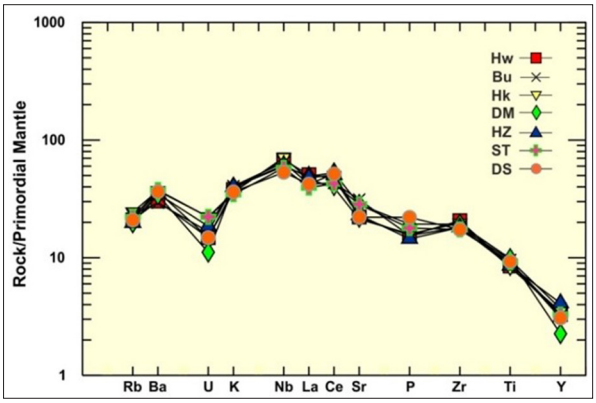

Figure 10. Spider diagram of incompatible elements from HI normalized to primitive mantle source. Elements are arranged in the order of their increasing incompatibility with the mantle rocks. The data are normalized to primordial mantle of Wood et al. (1979).

4.2.5 Tectonic Classification

The HI samples plot in the "within-plate" basalts and alkali field (Fig. 11a) on Ti/Y vs. Nb/Y discrimination plots (after Pearce, 1982). Pearce and Cann (1973) evaluated trace elements data on basalts from four major tectonic settings (Fig. 11b). The most of HI samples in this diagram plotting in "within-plate" basalts. The triangular diagram (Fig. 11c) with apices Zr/4, 2Nb and Y is suggested by Meschede (1986). All the HI samples situated in Al and All regions indicate the within-plate alkali basalt.

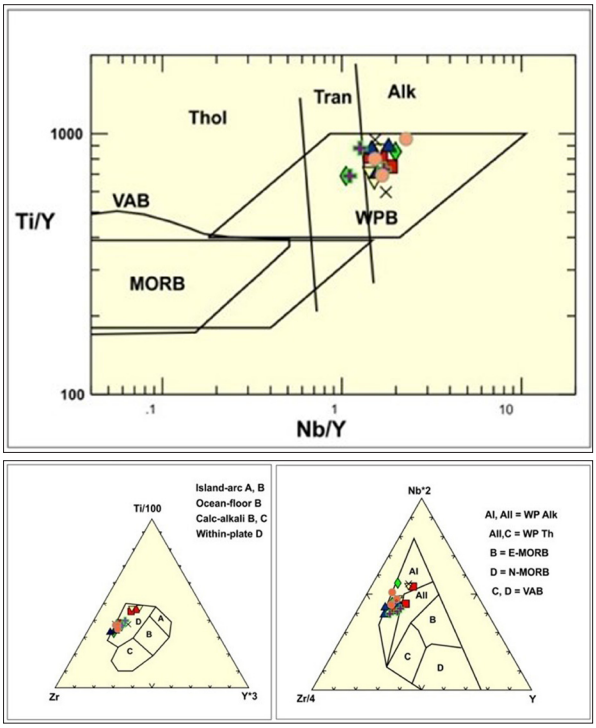

Figure 11. a. Ti/Y vs. Nb/Y discrimination diagram (after Pearce, 1982) displaying most HI samples plot between the alkalic and within-plate basalts. **b.** Zr, Ti/1000, and Y*3 tectonic discrimination diagram of the HI rocks (Pearce and Cann 1973). The HI samples fall in "within-plate" region. **c.** 2Nb – Zr/4 – Y discrimination diagram of Meschede (1986). AI: within-plate alkali basalts; AII: within-plate basalts and within- plate tholeiites; B: E-MORB; C: within-plate tholeiites and volcanic arc basalts; D: N-MORB volcanic arc basalts.

4.3 Petrogenesis of HI Samples

4.3.1 Crustal Contamination

The HI samples define a trend of constant La/ Nb compared with SiO_2 which can be imputed to the assimilation of low-La/Nb crustal contaminants during magma evolution (Walker et al., 2009). Mg# (MgO/ (MgO+FeO)) indicates the level of evolution of a volcanic rock (e.g. Basalt) since leaving its birth place (mantle). Mg# for the HI products ranges from 0.52 to 0.62 values, with an average of 0.57. These values are close to the values of 0.65, 0.77 and >0.70 for primary magmas reported by Wilson (1989) and Al-Malabeh (1994).

The primary nature of the magma, and the Mg#, provide an evidence for a closed-system magma chamber, and suggest that the contamination of the upper crust was minimal. Furthermore, the high K/Rb ratios, and the low Rb/Sr & K/Sr ratios in the HI rocks show a primary uncontaminated magmas (Al-Malabeh, 1994). Trace element modeling (Zr/Y vs. Ti/Y, Zr/Nb vs. La/Sm) indicates that the alkali HI samples were produced by a partial melting of an enriched mantle source that experienced little or no crustal contamination (Floyd et al., 2000).

4.3.2 Fractional Crystallization vs. Partial Melting

MgO contents (4-9 wt. %) were observed in all of the samples, demonstrating that they are close to primary magmas, and may have experienced minimal fractionation of mafic minerals such as olivine and pyroxene, which is consistent with the observed phenocrysts assemblages and argues for a rapid ascent from the mantle. The low Y content, high Zr/Y ratio, high TiO_2/Y ratio (Frey et al., 1978), and the high La/Yb ratio (Saunders et al., 1987) with averages of 20, support the idea that the studied rocks are derived from a mantle of garnet peridotite composition.

The REE pattern may help us illustrate a partial melting trend and a crystal fractionation trend for the HI rocks. The content of the incompatible elements, such as REE (See Fig. 9 and 10), in the melt decreases with increasing the degree of melting and decreasing the degree of fractional crystallization (Winter, 2001).

The negative K anomalies appearing in the more enriched profiles propose that for smaller degrees of partial melting, such K-bearing phases may have been held in the source, but they are depleted with a greater degree of partial melting (Ibrahim and others, 2014; Fitton and Dunlop, 1985; Smedley, 1988).

Because the slope on a REE diagram (See Fig. 9) is a function of F, the melt fraction (10 % partial melts) generated, the differences between HREE depletion and LREE enrichment are due to the low degrees of partial melting (Winter, 2001).

This result is propped by the Sr-Zr plot after Camp and Roobol (1989), where all samples (Fig. 12a) take place into a partial melting trend rather than proposing plagioclase fractionation (El-Hasan and Al-Malabeh, 2008).

4.3.3 Petrogenetic Modeling

The trace elements pattern of alkaline lavas is repeatedly explained as being due to low degrees of melt from a garnet peridotite source (Foulger et al., 2005). As mentioned earlier, a positive Nb peak is a good indicator that HI is a product of the asthenospheric part of the mantle rather than the lithospheric part. The high Ti/Y ratio and the stability of the Y content may indicate that the source magmas originated in garnet-bearing rocks.

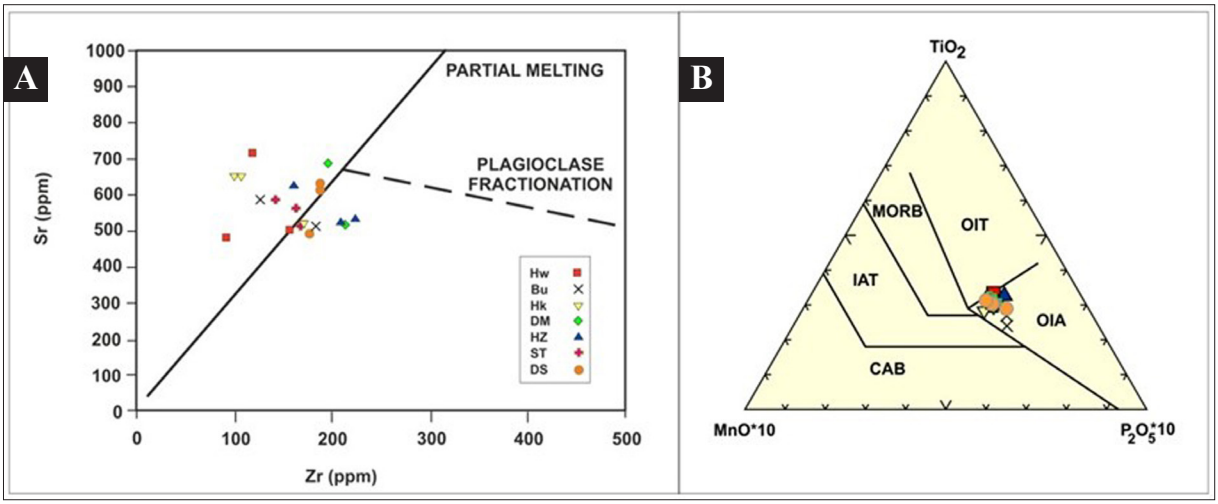

Figure 12. a. Plot of the HI samples on Sr-Zr diagram (Modified after Camp & Roobol, 1989) showing the limited plagioclase fractionation. **b.** MnO–TiO_2–P_2O_5 diagram (Mullen 1983) for the HI samples. (CAB: Calc-Alkaline Basalt, IAT: Island-Arc Tholeiites, MORB: Mid-Ocean Ridge Basalt, OIT: Ocean Island Tholeiites, OIA: Ocean Island Alkaline basalt).

Depending on Mullen (1983) discrimination diagram for basalts, MnO-TiO_2-P_2O_5 for the HI are compared with the oceanic island alkali basalts (OIA). The HI shows restricted major elements' ratios of the studied samples that fall within the range of OIBs (Fig. 12b). These results indicate that the HI samples cannot be created in a subcontinental lithosphere, but are generated from asthenospheric mantle (Al-Malabeh, 1994; Ibrahim et al., 2014).

Petrogenetic modeling of the HI samples depends primarily on the mantle plume activity. Morgan (1971) proposed that hotspot volcanism is produced by mantle plumes, involving the rapid ascent of uncommonly hot and floatable mantle materials from deep thermal boundary layers in the lower mantle (Fig. 13).

We conclude that there is a deeper possible partial source for the HI basalts at > 100 km (Al-Malabeh, 1994; Morgan, 1971). A basalt flow like those in HI has low silica contents and low viscosities so they can flow for long distances similar to Hawai'i (Bryant, 1991).

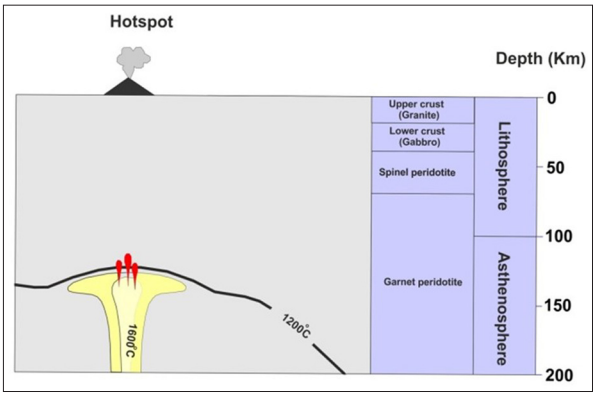

Figure 13. Structure of the crust and mantle below the HI source (After Al-Malabeh, 1994).

4. Conclusions

The basalt samples are characterized by a hypocrystalline texture and mesocratic colour index, Olivine- Plagioclase-Pyroxene Phyric Basalt (23 %), Olivine- Pyroxene Phyric Basalt (43 %) and Olivine Phyric Basalt (24 %). The microcrystalline matrix is dominated by plagioclase, augite, olivine and magnetite.

HI consists also of other accessory minerals such as nepheline and magnetite and secondary minerals such as carbonates, iddingsite and chlorite in addition to vesicles filled with gas bubbles and carbonates.

Porphyritic, Vesicular, Amygdaloidal, embayment, pilotaxitic, glomeroporphyritic and sub-ophitic are the major textures that emerged in basaltic samples in addition to some less visible textures such as seriate, ophitic, radiate and intergranular textures.

The typical evolutionary sequence in the alkaline series of the HI rocks starts with an alkali olivine basalt, and proceeds to become alkali trachy basalt and tephrite basanite.

The compositions of the HI samples plotted in highly undersaturated alkaline field, resulted from a primitive mantle source, situated in the within-plate alkali basaltic field and were produced by a lesser percentage of partial melting (about 10 %) of an enriched mantle source that experienced little or no crustal contamination.

Similarities between some OIB and continental basalts are another evidence of the asthenospheric source that resulted from mantle plumes producing melts called alkali HI that are very high in potassium and sodium.

References

Abed, A.M. (2000). Geology of Jordan. Jordanian Geologists Association, Amman.

Abu-Mahfouz, I., Al-Malabeh, A., and Rababeh, S. (2016). Geo-Engineering of Harrat Irbid Basaltic Rocks, Irbid District-North Jordan. Arabian Journal of Geosciences, 8(4): 231-248.

Al-Amoush, H. (2010). Integration of Vertical Electrical Sounding and Aeromagnetic Data Using GIS Techniques to Assess the Potential of Unsaturated Zone and Natural Basalt Caves for Groundwater Artificial Recharge in NE-Jordan. Jordan Journal of Civil Engineering, 4(4): 387-389.

Al-Malabeh, A. (2009). Cryptic Mantle Metasomatism: Evidences from Spinel l Herzolite Xenoliths/Al-Harida Volcano in Harrat Al-Shaam, Jordan. American Journal of Applied Sciences, 6(12): 2085-2092.

Al-Malabeh, A. (1994). Geochemistry of Two Volcanic Cones from the Intra- continental plateau Basalt of Harra El-Jabban, NE-Jordan. In Basaltic rocks of Various Tectonic Setting, Special Issue of the Geochemical Journal, Japan, 28: 542-558.

Al-Malabeh, A. (1993). The volcanolgy, mineralogy and geochemistry of selected pyroclastic cones from NE – Jordan and their evolution for possible industrial applications, p. 330.

Al-Oufi, A., Al-Malabeh, A., and Al-Tarazi, E. (2012). Characterization of Lava Caves, Using 2D Induced Polarization Imaging, Umm Al Quttein area, NE Jordan. 15th International Symposium on Vulcanospeleology, March 15-22, pp. 71-83.

Alexander, P., and Thomas, H. (2011). Copper In Deccan Basalts (India): Review Of the Abundance And Patterns Of Distribution. Boletín del Instituto de Fisiografía y Geología 79-81, pp. 107-112.

Anand, M., Taylor, L., Floss, C., Neal, C., Terada, K., and Tanikawa, S. (2006). Petrology and geochemistry of LaPaz Icefield 02205: A new unique low-Ti mare-basalt meteorite. Geochimica et Cosmochimica Acta, 70: 246–264.

Bryant, W.A. (1991). Likely Fault Zone, Lassen and Modoc counties. California Division of Mines and Geology Fault Evaluation Report 218.

Camp, V., and Roobol, M., (1989). The Arabian continental alkali province: Part I Evolution of Harrat Rahat, Kingdom of Saudi Arabia.Geological Society of. America Bulletin,101: 71-95.

El-Hasan, T., and Al-Malabeh, A. (2008). Geochemistry, Mineralogy and Petrogenesis of El-Lajjoun Pleistocene Alkali Basalt of Central Jordan. Jordan Journal of Earth and Environmental Sciences, 1(2): 53-62.

Fitton, J., and Dunlop, H. (1985). The Cameroon line, West Africa and its bearing on the origine of oceanic and continental alkali basalts. Earth and Planetary Science Letters, 72: 23–38.

Floyd, P., and Winchester, J. (1975). Magma Type and Tectonic Setting Discrimination using immobile trace elements. Earth Planetary Science Letters, 27: 211-218.

Floyd, P., Goncuoglu, M., Winchester, J., and Yaliniz, M. (2000). Geochemical Character and tectonic enviornment of Neotethyan ophiolitic fragments and metabasites in the Central Antolian Crystalline Complex, Turkey, in Bozkurt". Geological Special Publication, 173: 183-202.

Foulger, G., Natland, J., Presnall, D. and Anderson, D. (2005). Plates, Plumes, and Paradigms. Geological Society of America Special Papers, Vol. 388, p. 881.

Frey, F., Green, D., and Roy, S.D. (1978). Integrated Models of Basalt Petrogenesis - Study of Quartz Tholeiites to Olivine Melilities from South Eastern Australia Utilizing Geochemical and Experimental Petrological Data. Journal of Petrology, 19(3): 463-513.

Garfunkel, Z. (1989). Tectonic setting of Phanerozoic magmatism in Israel: Israel Journal of Earth Sciences, 38(2–4): 51–74.

Gill, R. (2010). Igneous Rocks and Processes: A Practical Guide. A John Wiley & Sons, Ltd., Publication, 2: 20-65.

Ibrahim, K. (1993): The geological framework for Harrat Ash – Shaam basaltic super group and its volcano tectonic evolution". Bulletin 25. NRA., Amman, Jordan.

Ibrahim, K., Rabba', I., and Tarawneh, K. (2001). Geological and mineral occurrences map of the northern Badia region, Jordan, scale 1:250,000. A Joint Report of the Higher Council for Science and Technology and the NRA, p. 136.

Ibrahim, K. Moh'd, B. Masri, A. Al-Taj, M. Musleh, S., and Alzughoul, K. (2014). Volcanotectonic evolution of central Jordan: Evidence from the Shihan Volcano. Journal of African Earth Sciences, 100: 541–553.

Illani, S., Harlvan, Y., Tarawneh, K., Rabba`, I., Weinberger, R., Ibrahim, K., Peltz, S., and Steinitz, G. (2001). Dating of the Harrat Ash – Shaam basalts ,Northeastern Jordan. Geological Society of America, Geology, 29(2): 171-174.

Irvine, T., and Barager, W. (1971). A guide to the chemical classification of the common rocks. Canadian Journal of Earth Sciences, 8: 523-548.

Kushiro, I. (1968). Compositions of magmas formed by partial zone melting of the earth's upper mantle. J. geophys. Res., 73: 619-634.

Le Bas, M., Le Maitre, R., Streckeisen, A., and Zanettin, B. (1986). A chemical classification of volcanic rocks based on the total alkalis-silica diagram. Journal of Petrology, 27: 745-750.

Meschede, M. (1986). A method of discriminating between different types of mid-ocean ridge basalts and continental tholeiites with the Nb-Zr-Y diagram. Chemical Geology, 56: 207-218.

Middlemost, E. (1975). The basalt clan. Earth Science Reviews, 11: 337-364.

Mo'hd, B. (1997). Geological Map of Irbid (3155II). 1:50,000, Natural Resources Authority, Amman, Jordan.

Morgan, J. (1971), Convection plumes in the lower mantle, Nature, 230: 42-43.

Mullen, E. (1983). MnO/TiO2/P2O5—a minor element discriminant for basaltic rocks of oceanic environments and implication for petrogenesis. Earth Planet. Sci. Lett., 62: 53–62.

Nakamura, N. (1974). Determination of REE, Ba, Fe, Mg, Na, and K in carbonaceous and ordinary chondrites. Geochim. Cosmochim. Acta, 38: 757–775.

Pearce, J. (1982). Trace element characteristics of lavas from destructive plate boundaries. In Andesites: Orogenic Andesites and Related Rocks (R.S. Thorpe, ed.). John Wiley & Sons, Chichester, U.K., pp. 525-548.

Pearce, J., and Norry, M. (1979). Petrogenetic implications of Ti, Zr, Y, and Nb variations in volcanic rocks. Contributions to Mineralogy and Petrology, 69(1): 33-47.

Pearce, J., and Cann, J. (1973). Tectonic setting of basic volcanic rocks determined using trace element analyses. Earth Planet. Sci. Lett., 19: 290–300.

Rittmann, A. (1957). On the serial character of igneous rocks. Egyptian Journal of Geology, 1: 23-48.

Rittmann, A. (1962). Volcanoes and their activity (translation P.A. Vincent). Interscience, New York, p. 305. Saunders, A., Rogers, G., Marriner, G., Terrell, D., and Verma, S. (1987). Geochemistry of Cenozoic volcanic rocks, Baja California, Mexico: Implications for the genesis of post-subduction magmas. Journal of Volcanology and Geothermal Research, 32: 223–245.

Smedley, P. (1988). Trace element and isotopic variations in Scottish and Irish Dinantian volcanism: evidence for an OIB-like mantle source. Journal of Petrology, 29: 413–443.

Sunkel, G. (1990). Origin of petrological and geochemical variations of Lau Basin Lavas (SW Pacific). Mar. Min., 9: 205–234.

Tarawneh, K. ShimonI, Rabba, I. Harlavan, Y. Peltz, S. Ibrahim, K. Weinberger, R., and Steinitz, G. (2000). "Dating Of the Harrat Ash Shaam Basalts/ NE Jordan (Phase 1)". NRA-GSI Report, p. 65.

Walker, R., Gans, P., Allen, M., Jackson, J., Khatib,M., Marsh, N., and Zarrinkoub, M. (2009). Late Cenozoic volcanism and rates of active faulting in eastern Iran. Geophys. J. Int., 177: 783–805.

Wilson, M. (1989). Igneous Petrogenesis, a Global Tectonic Approach. Unwin Hyman, London.

Winchester, J., and Floyd, P. (1976). Geochemical magma type discrimination: application to altered and metamorphosed basic igneous rocks. Earth Planet. Sei. Lett., 28: 459-469.

Winter, Ohn D. (2001). An Introduction to Igneous and Metamorphic Petrology. Library of Congress Cataloging-in-Publication Data, USA.

Wood, D., Tarney, J., Varet, J., Saunder, A., Bougault, H., Joron, J., Treuil, M., and Cann, J. (1979). Geochemistry of basalt drilled in the North Atlantic by IPOD leg 49. Implications for mantle heterogeneity. Earth and Planetary Science Letters, 42: 77-97.